PHYSICAL REVIEW B **87**, 054424 (2013)

Change of the optical conductivity spectra with orbital and spin ordering in spinel MnV_2O_4

T. Katsufuji,[1,2,*] T. Takubo,[1,†] and T. Suzuki[1,‡]

[1]*Department of Physics, Waseda University, Tokyo 169-8555, Japan*

[2]*Kagami Memorial Laboratory for Material Science and Technology, Waseda University, Tokyo 169-0051, Japan*

(Received 27 November 2012; published 19 February 2013)

Spinel MnV_2O_4 exhibits orbital ordering at $T_c = 57$ K accompanied by a structural phase transition from cubic to tetragonal and ferrimagnetic ordering. We measured the temperature dependence of the optical reflectivity spectra on the cleaved surface of a MnV_2O_4 single crystal with controlled twin structures below T_c. We found that there are two peaks at 1.6 and 2.3 eV, corresponding to the Mott excitations, in the optical conductivity spectra obtained by the Kramers-Kronig transformation of the reflectivity, and that the two peaks exhibit a similar anisotropic change below T_c. Furthermore, we found that these two peaks exhibit a different temperature dependence above T_c. We analyzed these results by a model in which the multiplet structures of the d state for the Mott excitation are fully taken into account, and discussed the occupation of the triply degenerate t_{2g} orbitals both below and above T_c.

DOI: 10.1103/PhysRevB.87.054424 PACS number(s): 75.25.Dk, 78.40.Ha, 71.70.Gm

I. INTRODUCTION

It is widely recognized that orbital ordering is a phenomenon observed in various transition-metal oxides. A typical example is seen in perovskite manganites,[1,2] where the degree of freedom arising from the twofold degeneracy in the e_g states of the Mn $3d$ orbitals orders in an antiferroic manner, namely, an electron occupies one of the two e_g states alternately in the Mn lattice. Several compounds are known to show the orbital ordering in the t_{2g} states of the d orbital with threefold degeneracy, for example, perovskite vanadates[3,4] and spinel vanadates.[5–13]

Various experimental techniques have been employed to study the orbital ordering in transition-metal oxides. Since orbital ordering is coupled with a lattice distortion, diffraction measurements are useful to detect the orbital ordering. It is known that resonant x-ray scattering can give more direct evidence of orbital ordering.[2] However, there have not been many studies so far about the electronic structure of the orbital ordered phase. One of the useful techniques to study the electronic structure is optical reflectivity measurement. In particular, the spectrum for the Mott excitation, i.e., the transition of an electron from one transition-metal site to another, can give the important information about the orbital states in transition metals.[14–25] For example, optical reflectivity measurements have been performed for perovskite RVO_3 (R is a rare earth) that exhibits the orbital ordering of V^{3+} ($3d^2$) at low temperatures.[15–18] Several peaks were observed in the optical conductivity spectra obtained by the Kramers-Kronig transformation of the reflectivity spectra, which arise from the Mott excitations with the multiplet structure of the final states. Drastic changes of these peaks are observed at the transition temperature of the orbital ordering, and the way of the spectral change depends on the types of orbital ordering, which are dominated by the size of the R ion.

It should be noted that the transition of the V electrons in the t_{2g} states to a different V ion occurs via the oxygen $2p$ state in perovskite RVO_3, and, thus, not only the orbital ordering but also the anisotropy of the transfer integrals arising from the so-called $GdFeO_3$-type distortion affects the Mott excitation in the optical conductivity spectra. In this regard, the orbital ordering in spinel vanadates AV_2O_4 (A is a divalent alkali earth) with V^{3+} ($3d^2$) is more suitable to the investigation of the electronic structure by the optical measurement since in this series of compounds, where VO_6 octahedra are edge sharing with each other, the transfer of the t_{2g} electrons occurs through the direct d-d transfer without the help of the O $2p$ state.

It is known that AV_2O_4 with various A^{2+} ions exhibits a structural phase transition into a tetragonal phase at low temperatures.[5–13] As to this phase transition, several theoretical models for the orbital ordering have been proposed: One is an antiferro-orbital (AFO) model proposed by Tsunetsugu and Motome,[26] where the first electron of $3d^2$ occupies the d_{xy} orbital and the second electron occupies the d_{yz} and d_{zx} orbital alternately along the c direction. Another model was proposed by Tchernyshyov,[27] which is a ferro-orbital (FO) model, where the first electron occupies the d_{xy} state and the second electron occupies the $d_{yz} + id_{zx}$ state at all the V ions. Experimentally, it was found by the x-ray diffraction measurement of a MnV_2O_4 single crystal, which exhibits a simultaneous ordering of spin and orbital (crystal structure) at 57 K, that the space group of the low-T phase is consistent with the Tsunetsugu-Motome–type orbital ordering.[8] It should be noted, however, that such an experimental result gives only the information of the symmetry in the orbital ordered state, but the number of electrons occupying each orbital is not known for the low-T phase of MnV_2O_4. Theoretically, the important role of the trigonal distortion in VO_6 octahedra was pointed out,[28,29] and it leads to the partial occupation of all the three t_{2g} states in the orbital ordered phase.

In this paper, we performed optical reflectivity measurements of MnV_2O_4. We found two peaks at 1.6 and 2.3 eV in the optical conductivity spectra, corresponding to the multiplet structures for the Mott excitation. We also found that these peaks exhibit anisotropic changes below the structural transition temperature ($T_c = 57$ K). The result was analyzed by the model that fully takes account of the multiplet structures in the final state of the Mott excitation.

II. EXPERIMENT

A single crystal of MnV_2O_4 was grown by the floating-zone method. We measured the reflectivity spectra both for the cleaved and the polished surfaces, and found that the results are discernibly different between the two. It is known that

the remnant stress in the polished surface affects the optical spectra, and often suppresses the spectral change associated with a phase transition that is strongly coupled with lattice distortion.[30] Therefore, we show the optical reflectivity spectra for the cleaved surface along the (001) plane, which was confirmed by the Laue method, in the following. The size of the sample was ∼5 × 5 mm along the surface and ∼1 mm in thickness.

One of the problems when measuring the polarization dependence of the optical spectra for the sample that exhibits a structural phase transition with symmetry lowering is the formation of twin structures. This is the case for the present MnV_2O_4, which exhibits a structural phase transition from cubic to tetragonal. We found that, because of the difference in the thermal contraction, the ab plane of the crystal is preferably oriented when it was attached to the glass plate, whereas the ac plane is when attached to the copper plate. Thus, by measuring the spectra for the sample on both plates, we can obtain both the spectra with the polarization along the a and c axes in the tetragonal phase.

Optical reflectivity measurements were performed with a grating spectrometer (Bunkoukeiki M25) between 0.7 and 5 eV for the temperature range between 300 and 5 K using a He-gas-flow cryostat. For the Kramers-Kronig transformation, we assume a constant reflectivity above 5 eV up to 8 eV, and the ω^{-4} extrapolation was used above 8 eV. The reflectivity below 0.7 eV was extrapolated by a constant reflectivity.

III. EXPERIMENTAL RESULTS

Figures 1(a) and 1(b) show the reflectivity spectra at various temperatures (T) for (a) $T > T_c$ and (b) $T < T_c$. As can be seen, a large peak at ∼1.5 eV and a smaller peak at 2.2 eV are observed in the reflectivity spectra between 1 and 3 eV. The peak at 1.5 eV grows with decreasing T above $T_c = 57$ K,

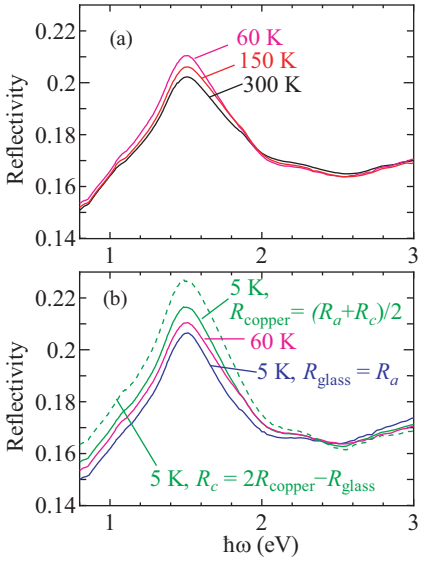

FIG. 1. (Color online) Optical reflectivity spectra for MnV_2O_4 (a) above $T_c = 57$ K and (b) at 60 K ($>T_c$) and 5 K ($<T_c$) on a glass plate ($R_{glass} = R_a$) and copper plate [$R_{copper} = (R_a + R_c)/2$]. R_c at 5 K obtained as $2R_{copper} - R_{glass}$ is also plotted by a dashed line in (b).

whereas the peak at 2.2 eV is suppressed with decreasing T [Fig. 1(a)]. Below T_c in the tetragonal phase, both peaks further grow for the sample attached to a copper plate, whereas both are suppressed for the sample attached to a glass plate [Fig. 1(b)]. As discussed above, the spectrum for the sample on the glass plate (R_{glass}) corresponds to the reflectivity with the polarization along the a axis of the tetragonal phase (R_a), whereas the spectrum for the sample on the copper plate (R_{copper}) is the sum of that with the polarization along the a axis (R_a) and c axis (R_c).

We measured the polarization dependence of the reflectivity spectra for the sample on the copper plate, but barely found the difference for the different directions of the polarization. This means that the domain size of the tetragonal phase is smaller than the spot size of the incident light ($\phi \sim 1$ mm), and the c and a axes are randomly oriented along the surface of the sample attached to a copper plate. Thus, by measuring the reflectivity spectra without a polarizer, and assuming that the domain size of the tetragonal phase is much larger than the wavelength of the light (∼1 μm), R_{copper} is given by $(R_a + R_c)/2$. Accordingly, R_c is given by $2R_{copper} - R_{glass}$, which is plotted by a dashed line in Fig. 1(b).

Figures 2(a) and 2(b) show the optical conductivity spectra [$\sigma(\omega)$] obtained from the Kramers-Kronig transformation of the reflectivity spectra $R_a(\omega)$ and $R_c(\omega)$. There are two structures at 1.6 and 2.3 eV. The 1.6-eV peak grows with decreasing T above T_c, and below T_c, both the 1.6 and 2.3 eV peaks grow in the optical conductivity along the c axis [$\sigma_c(\omega)$], whereas they are suppressed in that along the a axis [$\sigma_a(\omega)$]. To see the T dependence more clearly, we take the difference of the $\sigma(\omega)$ spectra at two different temperatures, as shown in Fig. 3. The 2.3-eV peak seems to be suppressed with decreasing T above T_c.

To obtain the spectral weight for the two peaks in the $\sigma(\omega)$ spectra, we fit the $\sigma(\omega)$ spectra with five Lorentzians, as shown in Fig. 4(a). The sum of the two Lorentzians with the lowest frequencies $I_0 + I_1$ corresponds to the 1.6-eV peak[31] and the

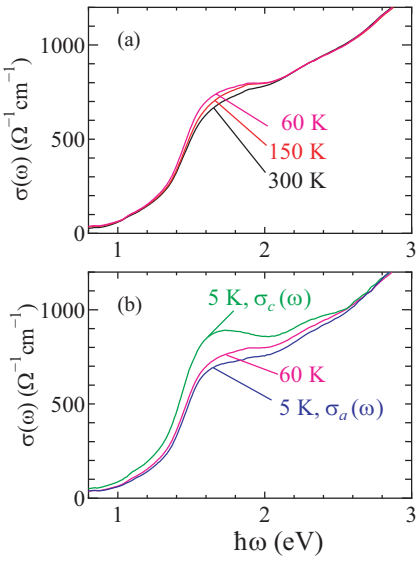

FIG. 2. (Color online) Optical conductivity spectra for MnV_2O_4 (a) above $T_c = 57$ K and (b) at 60 K ($>T_c$) and 5 K ($<T_c$) along the a and c axis [$\sigma_a(\omega)$ and $\sigma_c(\omega)$].

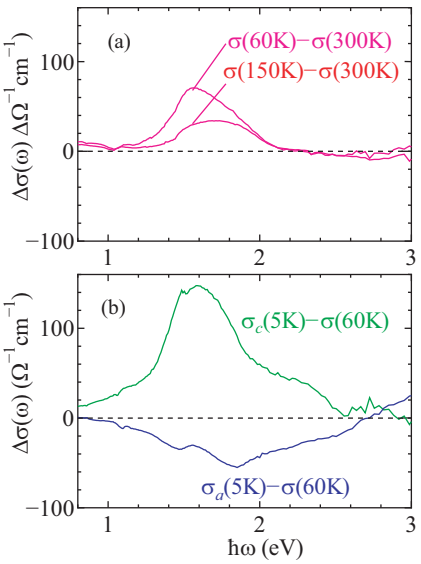

FIG. 3. (Color online) The difference of the optical conductivity spectra for MnV_2O_4 (a) between two temperatures above $T_c = 57$ K and (b) between 5 K [$<T_c$, $\sigma_a(\omega)$ and $\sigma_c(\omega)$] and 60 K ($>T_c$).

third one I_2 to the 2.3-eV peak. The remaining two correspond to the structures at higher frequencies. Figure 4(b) shows the T dependence of the spectral weight for $I_0 + I_1$ and I_2. As can be seen, the spectral weight for the 1.6-eV peak ($I_0 + I_1$) gradually increases with decreasing T above T_c, and below T_c, the spectral weight for σ_c sharply increases whereas that for σ_a decreases. The spectral weight for the 2.3-eV peak

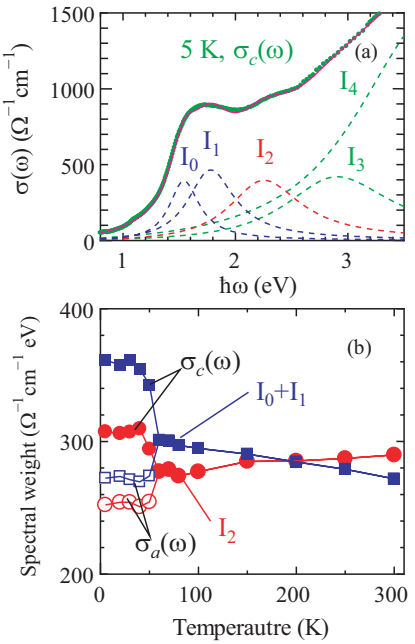

FIG. 4. (Color online) (a) An example of the fitting for the $\sigma_c(\omega)$ spectrum at 5 K. The dotted line is the experimentally obtained $\sigma_c(\omega)$ and the solid line is the fitting curve. Dashed lines correspond to each Lorentzian. (b) Temperature dependence of the spectral weight for $I_0 + I_1$ (1.6-eV peak) and that for I_2 (2.3-eV peak). Closed symbols correspond to that for $\sigma_c(\omega)$ and open symbols to that for $\sigma_a(\omega)$ below $T_c = 57$ K.

(I_2) gradually decreases with decreasing T above T_c, and the behavior below T_c is similar to that for the 1.6-eV peak.

Similar structures were observed in the $\sigma(\omega)$ spectra for perovskite RVO_3 with V^{3+} ($3d^2$) around 2 eV.[15–18] For example, three peaks at 1.8, 2.4, and 3.3 eV were observed in YVO_3, which exhibits a peculiar dependence on the orbital and spin ordering, and those peaks were assigned to Mott excitations with multiplet structures.[16] Thus, it is reasonable to assign the two peaks at 1.6 and 2.3 eV in the present compound to the same origin. To understand the T dependence of them both below and above T_c, we need to consider how the spectral weight of each multiplet structure for the Mott excitation is dominated by the orbital and spin ordering. We discuss this issue in the following section.

IV. ANALYSIS OF THE OPTICAL SPECTRA

There are several papers so far published that discuss the Mott excitation in the optical spectra based on the electronic structure of the d^n state for the transition-metal oxides.[14–18,20] However, the multiplet structure of the d^{n+1} state is not fully taken into account there. Namely, if one electron moves from one site to another site and it becomes a d^{n+1} state, the state is usually not an eigenstate (multiplet) of the d^{n+1} state but a superposition of them. Furthermore, the present compound exhibits a noncollinear spin structure below T_c,[9] and that needs to be considered in the analysis of the optical spectra. In the following and Appendixes, the correct treatment of the multiplets and spin structures for the Mott excitation in the optical spectra is discussed based on the theory of the multiplets in transition-metal ions.[32]

Here, we take account of the t_{2g} states and the Coulomb interaction between the two electrons in the t_{2g} states on the same site. The transfer of the electrons to a different site is ignored except for (1) as a second-order perturbation when considering the orbital-orbital interaction, and (2) as a current operator when considering the optical excitation process (see Appendix A). The ground state is thus given by the multiplet of the d^2 configuration in the t_{2g} state with the lowest energy $^3T_1$ with the ninefold degeneracy (3 by the orbital and 3 by the spin).[32] For example, the 3 states with $S_z = 1$ of $^3T_1$ are $|d_{xy}d_{yz}|$, $|d_{yz}d_{zx}|$, and $|d_{zx}d_{xy}|$, where d_{xy} means that the d_{xy} state is occupied by an up-spin electron, and $|\ldots|$ indicates the Slater determinant.

Associated with the Mott excitation, one site (the A site) becomes the d^1 configuration, whereas another site (the B site) becomes the d^3 configuration. The eigenstates of the d^3 configuration in the t_{2g} states are classified into four multiplets with the following irreducible representation $^4A_2$ (fourfold degeneracy, the energy is $3U' - 3J$), ^2E (fourfold, $3U'$), $^2T_1$ (sixfold, $U + 2U' - 2J$), and $^2T_2$ (sixfold, $U + 2U'$). U and U' are the Coulomb integral between the same and different orbitals in the t_{2g} states, respectively, and J is the exchange integral for the t_{2g} states. It should be noted that the energy of the $^3T_1$ state for the d^2 configuration is given by $U' - J$ in this notation.

The frequency of the peak in the optical spectrum is given by the difference in the energy of the final and initial states $\varepsilon_f - \varepsilon_0$. ε_0 is twice the energy of the $^3T_1$ state in the d^2 configuration, whereas ε_f is the energy of the d^3 state (since the interaction of the d^1 state is zero). Thus, $\hbar\omega = \varepsilon_f - \varepsilon_0$ for $^4A_2$, ^2E, $^2T_1$,

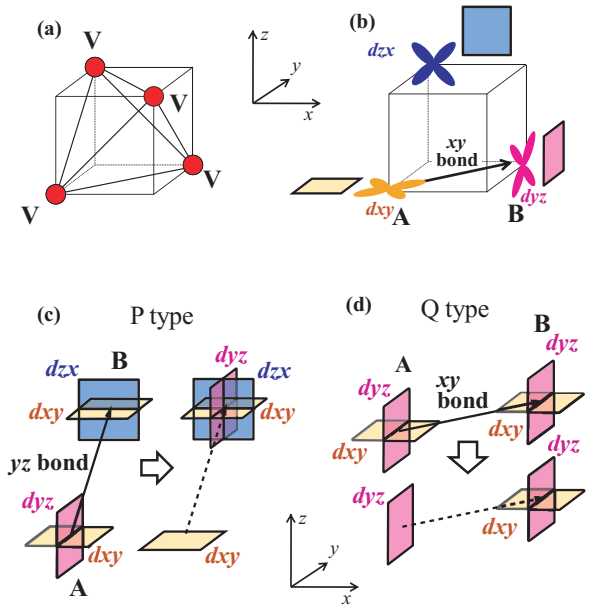

FIG. 5. (Color online) (a) Arrangement of the V ions in MnV_2O_4. (b) Three t_{2g} orbitals, each of which is represented by a square parallel to the orbital plane. The arrow represents an xy bond. (c) Example of the P-type orbital relation. (d) Example of the Q-type orbital relation.

and ${}^2T_2$ is $U'-J$, $U'+2J$, U, and $U+2J$, respectively. In the atomic d orbitals, there is a relation $U'=U-2J$, and $\hbar\omega$ becomes $U-3J$, U, U, $U+2J$.

In MnV_2O_4 with a spinel structure, V ions are located on the corner of a tetrahedron, as shown in Fig. 5(a). We take account of only a direct d-d transfer between the neighboring V sites for the optical excitation. In this case, any bond AB is on the edge of the tetrahedron, and if a bond AB is specified, only the electrons in one specific orbital at the A site can move to the B site. For example, if a bond AB is on the xy plane, 45° away from the x axis ("xy bond"), as illustrated in Fig. 5(b), only the d_{xy} electron at the A site can move to the B site, but the d_{yz} and d_{zx} electrons can not.

In such a case, the orbital relations for all the bonds can be classified into three types: One is the case where an electron at the A site can move to the unoccupied state at the B site; for example, the orbital state at the A site is $d_{xy}d_{yz}$, that at the B site is $d_{zx}d_{xy}$, and AB is connected by the yz bond, as shown in Fig. 5(c). We call this type as a "P-type" orbital relation. Second is the case where an electron at the A site can move to an occupied state at the B site; for example, the orbital state at the A site is $d_{xy}d_{yz}$, that at the B site is $d_{xy}d_{yz}$, and AB is connected by the xy bond, as shown in Fig. 5(d), which we call a "Q-type" relation. The third is the case where no electron at the A site can move to the B site, which can be ignored in the calculation of the Mott excitation spectrum.

We define $I_{\vec{e}}(\Gamma)$ as the intensity of the optical spectrum corresponding to the excitation to the d^3 state given by the irreducible representation $\Gamma = {}^4A_2$, ${}^2E$, ${}^2T_1$, and ${}^2T_2$ when the polarization of the light is $\vec{e}$. With a simple calculation (see Appendix A), it can be shown that this $I_{\vec{e}}(\Gamma)$ is given by the following formula:

$$I_{\vec{e}}(\Gamma) = \sum_{\mu}\sum_{\lambda}(\vec{e}\cdot\vec{r}_{\mu})^2 p(\mu,\lambda) I^{\lambda}_{\theta_{\mu}}(\Gamma), \tag{1}$$

where μ specifies which V-V bond is, λ specifies the type of orbital relation (P or Q), and $\vec{r}_{\mu}$ is the unit vector along the μ bond. $p(\mu,\lambda)$ corresponds to the probability that the orbital relation for the bond μ is λ (= P or Q) type. $I^{\lambda}_{\theta_{\mu}}(\Gamma)$ is the transition probability to the Γ state when the orbital relation is λ (= P or Q) type, and the relative angles between the spins on the ends of the bonds (at the A and B sites) is θ_{μ}. It should be noted that we have to count both the A→B transition and B→A transition in the μ (bond) summation.

Specific formulas of $I^{\lambda}_{\theta_{\mu}}(\Gamma)$ do not depend on the orbital-ordering pattern, and can be calculated based on the electronic state of each irreducible representation, as discussed in the Appendix B. The results are as follows:

$$\begin{aligned} I^{\mathrm{P}}_{\theta}({}^4A_2) &= |\alpha(\theta)|^2 + \tfrac{2}{3}|\beta(\theta)|^2 + \tfrac{1}{3}|\gamma(\theta)|^2, \\ I^{\mathrm{P}}_{\theta}({}^2E) &= \tfrac{1}{3}|\beta(\theta)|^2 + \tfrac{2}{3}|\gamma(\theta)|^2, \\ I^{\mathrm{Q}}_{\theta}({}^2T_1) &= \tfrac{1}{4}|\beta(\theta)|^2 + \tfrac{1}{2}|\gamma(\theta)|^2, \\ I^{\mathrm{Q}}_{\theta}({}^2T_2) &= \tfrac{1}{4}|\beta(\theta)|^2 + \tfrac{1}{2}|\gamma(\theta)|^2, \end{aligned} \tag{2}$$

and $I^{\mathrm{P}}_{\theta}({}^2T_1) = I^{\mathrm{P}}_{\theta}({}^2T_2) = I^{\mathrm{Q}}_{\theta}({}^4A_2) = I^{\mathrm{Q}}_{\theta}({}^2E) = 0$. $\alpha(\theta)$, $\beta(\theta)$, and $\gamma(\theta)$ are determined by the following relations:

$$\begin{aligned} &\alpha(\theta) : \beta(\theta) : \gamma(\theta) = \frac{1}{1-\cos\theta} : \frac{\sqrt{2}}{\sin\theta} : \frac{1}{1+\cos\theta}, \\ &|\alpha(\theta)|^2 + |\beta(\theta)|^2 + |\gamma(\theta)|^2 = 1. \end{aligned} \tag{3}$$

In order to obtain $p(\mu,\lambda)$ and discuss the spectral weight $I_{\vec{e}}(\Gamma)$ in Eq. (1), we need to assume some orbital-ordering pattern. Here, we consider the orbital ordering where the probability of the orbital occupancy at each site is given as shown in Fig. 6, which is consistent with the space group $I4_1/a$ experimentally obtained.[8] When $a=b=0$, this orbital state becomes the Tsunetsugu-Motome phase (AFO phase). The orbital state proposed by Tchernyshyov (FO phase) corresponds to $a=0$ and $b=\frac{1}{2}$. When $a=b=\frac{1}{3}$ and $|\alpha(\theta)|^2$, $|\beta(\theta)|^2$, and $|\gamma(\theta)|^2$ in Eq. (2) are all set as $\frac{1}{3}$, it becomes a paramagnetic phase with no orbital ordering.

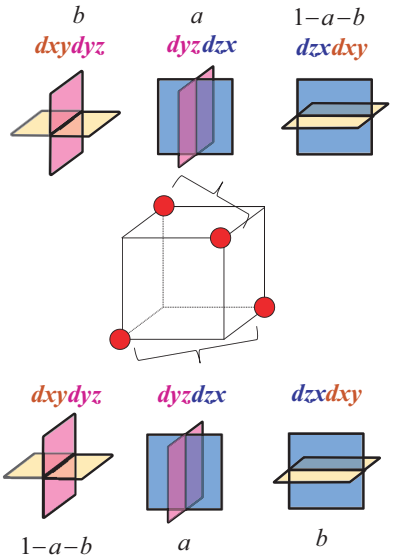

FIG. 6. (Color online) Probability of the orbital occupancy for the orbital ordering assumed in this study.

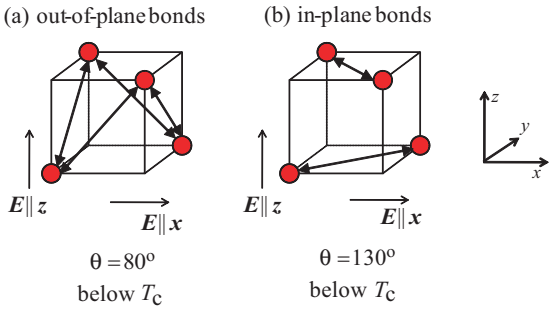

FIG. 7. (Color online) (a) Out-of-plane and (b) in-plane bonds shown by arrows, which are defined based on the orbital ordering in Fig. 6.

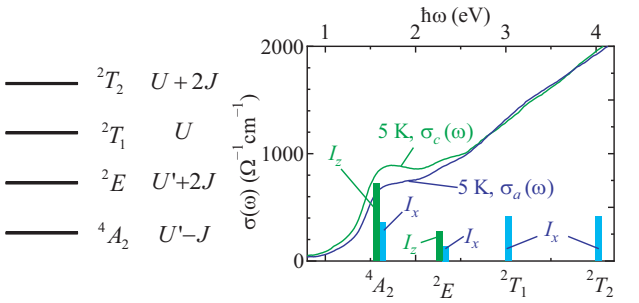

FIG. 8. (Color online) (Left) Schematic illustration of the Mott excitations with the multiplets of the d^3 final state, and (right) correspondence between the optical conductivity spectra in the experiment (solid lines) and the $^4A_2$ and ^2E excitations (bars). The bars for the $^2T_1$ and $^2T_2$ excitations only give a possible correspondence to the spectra with small peaks above 3 eV.

When we take the μ (bond) summation in this orbital state, it is enough to consider the bonds shown in Fig. 7; there are 12 bonds in total (counting both back and forth directions), and those are classified into 8 out-of-plane bonds and 4 in-plane bonds. It is easy to calculate the probability $p(\mu,\lambda)$ for each bond. (The details and results are described in the Appendix C.)

According to the neutron scattering measurement below T_c,[9] the relative angle of the V spins on the ends of the out-of-plane bond is $\theta = 80^\circ$, and that of the in-plane bond is $\theta' = 130^\circ$. With these discussions, we can calculate the specific values of $I_x(\Gamma)$ and $I_z(\Gamma)$, where $\vec{e} \parallel x$ and $\vec{e} \parallel z$, respectively.

For the Tsunetsugu-Motome phase (AFO phase, $a = b = 0$) with the spin structure experimentally obtained ($\theta = 80^\circ$ and $\theta' = 130^\circ$), the result is as follows: $I_x(^4A_2) \sim 0.72$, $I_x(^2E) \sim 0.28$, $I_x(^2T_1) \sim 0.82$, $I_x(^2T_2) \sim 0.82$, and $I_z(^4A_2) \sim 1.45$, $I_z(^2E) \sim 0.55$, $I_z(^2T_1) = I_z(^2T_2) = 0$ (Table I). By comparing this with the spectral weight of each peak and its anisotropy in the experimentally obtained optical conductivity spectra, as illustrated in Fig. 8, it is reasonable to assign that the peak at 1.6 eV in the experiment corresponds to the excitation to the $^4A_2$ state ($I_z = 1.45$ and $I_x = 0.72$ in the calculation), 2.3 eV to the ^2E state ($I_z = 0.55$ and $I_x = 0.28$), and the structures at higher energies to the $^2T_1$ and $^2T_2$ states. Two issues should be noted in this regard: (1) The charge-transfer excitation from the oxygen $2p$ to V $3d$ state is likely to be superposed to the higher-energy structures above 3 eV. (2) The ^2E and $^2T_1$ states are energetically degenerate with the relation $U' = U - 2J$, but it is likely that this degeneracy is lifted in the present compound, probably due to the hybridization of the t_{2g} states with the $2p$ states of the neighboring oxygen ions.

For the paramagnetic phase with no orbital ordering [$a = b = \frac{1}{3}$ and $|\alpha(\theta)|^2 = |\beta(\theta)|^2 = |\gamma(\theta)|^2 = \frac{1}{3}$], $I(^4A_2) = \frac{16}{27} \sim 0.59$, $I(^2E) = \frac{8}{27} \sim 0.30$, and $I(^2T_1) = I(^2T_2) = \frac{4}{9} \sim 0.44$

TABLE I. Calculated spectral intensity $I_{\vec{e}}(\Gamma)$ for the AFO, FO, and paramagnetic phases with no orbital ordering.

		$^4A_2$	^2E	$^2T_1$	$^2T_2$
AFO	I_x	0.72	0.28	0.82	0.82
	I_z	1.45	0.55	0	0
FO	I_x	0.36	0.14	0.92	0.92
	I_z	0.72	0.28	0.21	0.21
Para	I	0.59	0.30	0.44	0.44

(Table I). Thus, if the system exhibits a phase transition from the paramagnetic phase with no orbital ordering to the Tsunetsugu-Motome phase, the spectral weight of the 1.6-eV peak ($^4A_2$) should increase both in the $\sigma_a(\omega)$ and $\sigma_c(\omega)$ spectra below T_c. Experimentally, however, the spectral weight increases only in $\sigma_c(\omega)$, but it decreases in $\sigma_a(\omega)$.

We also consider the FO phase proposed by Tchernyshyov ($a = 0$ and $b = \frac{1}{2}$) with the spin structure experimentally obtained ($\theta = 80^\circ$ and $\theta' = 130^\circ$) and the result is as follows: $I_x(^4A_2) \sim 0.36$, $I_x(^2E) \sim 0.14$, $I_x(^2T_1) = I_x(^2T_2) \sim 0.92$, and $I_z(^4A_2) \sim 0.72$, $I_z(^2E) \sim 0.28$, $I_z(^2T_1) = I_z(^2T_2) = 0.21$ (Table I). Thus, if the system exhibits a phase transition from the paramagnetic phase with no orbital ordering to the Tchernyshyov phase, the 2.3-eV peak (^2E) should be suppressed both in the $\sigma_a(\omega)$ and $\sigma_c(\omega)$ spectra below T_c. This is not consistent with the experimental result.

To reconcile the experimental result and calculation, we take account of the orbital state in-between the Tsunetsugu-Motome and Tchernyshyov phases; namely, the first electron occupies the d_{xy} state and the second electron occupies the $d_{yz} + i\zeta d_{zx}$ or $d_{zx} + i\zeta d_{yz}$ ($0 \leqslant \zeta \leqslant 1$) state alternately along the c axis. In this case, $a = 0$ and $0 \leqslant b \leqslant \frac{1}{2}$, where b is

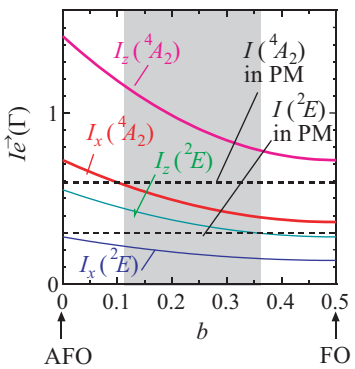

FIG. 9. (Color online) The value of $I_{\vec{e}}(\Gamma)$ below T_c (shown by solid curves) as a function of b. a is fixed to 0. The left end corresponds to the Tsunetsugu-Motome AFO phase, whereas the right end to the Tchernyshyov FO phase. The dashed lines indicate the value of $I_{\vec{e}}(\Gamma)$ above T_c. The shaded area ($0.12 < b < 0.36$) corresponds to the one that is qualitatively consistent with the experimental result.

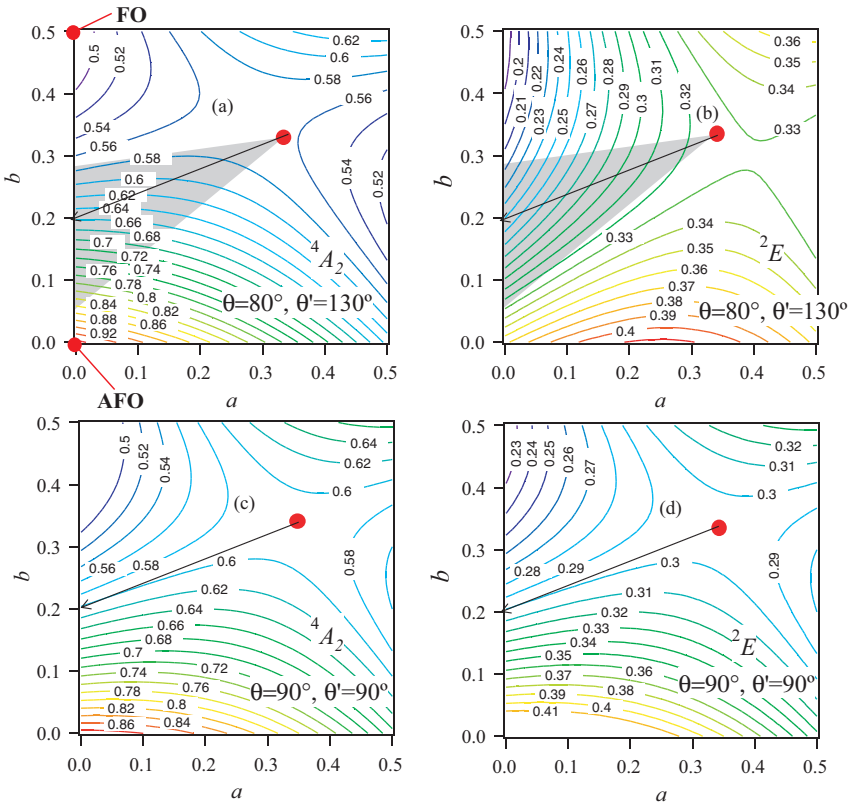

FIG. 10. (Color online) Contour map of $I_{\vec{e}}(\Gamma)$ in the cubic phase as a function of a and b for $\Gamma =$ (a) $^4A_2$ with $\theta = 80^\circ$ and $\theta' = 130^\circ$, (b) ^2E with $\theta = 80^\circ$ and $\theta' = 130^\circ$, (c) $^4A_2$ with $\theta = \theta' = 90^\circ$, and (d) ^2E with $\theta = \theta' = 90^\circ$. For the shaded area in (a) and (b), see text.

given by $b = \zeta^2/(1+\zeta^2)$. As seen in Fig. 9, to reproduce the experimental results, in which both the 1.6- and 2.3-eV peaks grow in $\sigma_c(\omega)$ but are suppressed in $\sigma_a(\omega)$, b needs to be between 0.12 and 0.36 (the shaded area in Fig. 9).

We also discuss the T dependence of the spectral weight for each peak above T_c; i.e., experimentally, the spectral weight of the 1.6-eV peak increases, whereas that of the 2.3-eV peak decreases with decreasing T. Since the spectral weight in the present model depends only on the orbital relation and relative angle of the spins at the ends of the V-V bonds, we can calculate the peak intensity of the state without long-range ordering by considering the correlation of the orbitals and spins as the deviation of a and b from $\frac{1}{3}$, and $|\alpha(\theta)|^2$, $|\beta(\theta)|^2$, and $|\gamma(\theta)|^2$ from $\frac{1}{3}$. Here, we assume the anisotropic correlation of the orbitals and spins as shown in Fig. 6, and calculate the intensity in the cubic phase by taking the average of I_x and I_z as

$$I(\Gamma) = \tfrac{2}{3} I_x(\Gamma) + \tfrac{1}{3} I_z(\Gamma). \tag{4}$$

First, if we keep the spins uncorrelated, i.e., $|\alpha(\theta)|^2 = |\beta(\theta)|^2 = |\gamma(\theta)|^2 = \frac{1}{3}$ and only change the orbital correlations a and b, $I(^4A_2)/I(^2E)$ is always 2, and thus, the different T dependence of the 1.6- and 2.3-eV peaks can not be explained. On the contrary, if we keep the orbitals uncorrelated, i.e., $a = b = \frac{1}{3}$, and only change the spin correlation θ (the angle between the spins on the out-of-plane bond) and θ' (that on the in-plane bond), the increase of the 1.6-eV peak and the decrease of the 2.3-eV peak can be reproduced if both θ and θ' decrease from 90°, namely, the enhancement of the ferromagnetic correlation. However, it is unlikely that such an isotropic ferromagnetic spin correlation is enhanced above T_c without orbital ordering or correlation.

Therefore, the most likely interpretation for the T dependence of the 1.6- and 2.3-eV peaks above T_c is that both the spin and orbital correlations are enhanced with decreasing T. Figure 10 shows the contour map of the spectral intensity for the $^4A_2$ and ^2E peak as a function of a and b when $\theta = 80^\circ$ and $\theta' = 130^\circ$ [Figs. 10(a) and 10(b)] and $\theta = \theta' = 90^\circ$ [Figs. 10(c) and 10(d)]. As can be seen in Figs. 10(a) and 10(b), where $\theta = 80^\circ$ and $\theta' = 130^\circ$ are fixed, if we start from the position $a = b = \frac{1}{3}$ (without orbital correlation), the shaded area corresponds to the direction along which the intensity of the $^4A_2$ peak increases and that of the ^2E peak decreases. When $\theta = \theta'$ is fixed as 90° [Figs. 10(c) and 10(d)], this direction approximately corresponds to that along which the intensity of both the $^4A_2$ and ^2E peaks remain unchanged.

Thus, let us assume that the orbital occupancy parameters (a and b) and spin angles (θ and θ') are simultaneously changed as follows:

$$\theta = 90 - 10\tau, \quad \theta' = 90 + 40\tau, \quad a = \frac{1}{3}(1-\tau), \quad b = \frac{1}{3} - \left(\frac{1}{3} - 0.2\right)\tau, \tag{5}$$

where τ ($0 \leqslant \tau \leqslant 1$) is a parameter that is supposed to vary with T. $\tau = 0$ corresponds to the state with no spin and no orbital correlation, and $\tau = 1$ to the fully correlated spin ($\theta = 80^\circ$ and $\theta' = 130^\circ$) and orbital ($a = 0$ and $b = 0.2$). The change of $I(^4A_2)$ and $I(^2E)$ with τ is plotted in Fig. 11. In the same figure, the value of $I_x(^4A_2)$, $I_z(^4A_2)$, $I_x(^2E)$, $I_z(^2E)$ with

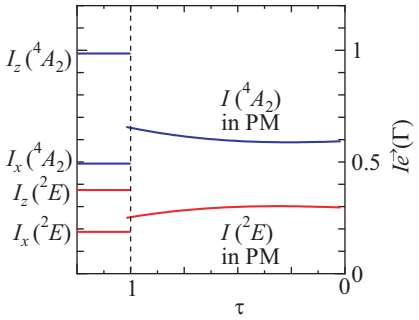

FIG. 11. (Color online) $I_{\vec{e}}(\Gamma)$ in the cubic phase for $\Gamma = I(^4A_2)$ and $I(^2E)$ by Eq. (5) as a function of τ. τ increases toward left in the figure to easily see the correspondence with the experiment [Fig. 4(b)]. In the left, $I_{\vec{e}}(\Gamma)$ in the tetragonal phase is plotted.

$\theta = 80^\circ$, $\theta' = 130^\circ$, $a = 0$, and $b = 0.2$ is also plotted in the left.

On the basis of this result, the T and polarization dependencies of the $\sigma(\omega)$ spectra can be possibly explained as follows: Above T_c, both the orbital occupancy parameters (a and b) and spin angles (θ and θ') gradually deviate from the values for no correlation ($a = b = \frac{1}{3}$ and $\theta = \theta' = 90^\circ$) and approach the values of the ground state ($a = 0$, $b = 0.2$, $\theta = 80^\circ$, and $\theta' = 130^\circ$) with decreasing T in the cubic phase [corresponding to the increase of τ from 0 to 1 in Eq. (5)]. Below T_c, the anisotropy of the crystal appears and the $\sigma(\omega)$ along the a and c become different. It should be emphasized that the value $b = 0.2$ in the ground state, which reproduces the increase of $I(^4A_2)$ and decrease of $I(^2E)$ with increasing τ (decreasing T above T_c) best, is within the range of $0.12 < b < 0.36$, which was determined independently from how the anisotropy appears below T_c, as shown in Fig. 9. This consistency supports the applicability of the present model to the optical conductivity spectra for MnV_2O_4.

V. SUMMARY

We measured the optical reflectivity spectra on the cleaved surface of spinel MnV_2O_4, which exhibits orbital ordering at $T_c = 57$ K. We found that two peaks at 1.6 and 2.3 eV exist in the optical conductivity spectra obtained by the Kramers-Kronig transformation of the reflectivity spectra. These can be assigned to the Mott excitations, where one electron moves from one V site ($3d^2 \rightarrow 3d^1$) to the next V site ($3d^2 \rightarrow 3d^3$). We found that the 1.6-eV peak grows, whereas the 2.3-eV peak is suppressed with decreasing T above T_c. We also found that both peaks grow in the optical conductivity spectra along the c axis in the tetragonal phase below T_c, whereas they are suppressed in those along the a axis. We analyzed the data by a model in which the multiplet structures of the final state are fully taken into account, and found that the change of the two peaks below T_c can be reproduced by assuming that the ground state below T_c is that between the antiferro-orbital phase proposed by Tsunetsugu and Motome and the ferro-orbital phase proposed by Tchernyshyov. We also found that the change of the two peaks with decreasing T above T_c can be reproduced by assuming that the orbital and spin correlation is enhanced as if the system approaches the ground state with decreasing T even above T_c.

ACKNOWLEDGMENTS

We thank M. Katsumura, M. Ryose, and T. Omura for their help in growing single crystals. This work was supported by a Grant-in-Aid for Scientific Research B (21340105) from JSPS.

APPENDIX A: OPTICAL CONDUCTIVITY SPECTRA FOR MOTT EXCITATIONS

In this Appendix, we discuss the details in the treatment of the Mott excitation with multiplet structures in the optical conductivity spectrum. This is a straightforward but a little tedious discussion. Still, it can be applied to the Mott excitations in the optical conductivity spectra for other compounds.

In general, the optical conductivity spectrum is given by the following formula[33]:

$$S_{\vec{e}}(\omega) = \sum_f |\langle f|\vec{e}\cdot\vec{J}|0\rangle|^2 \delta[\hbar\omega - (\varepsilon_f - \varepsilon_0)], \qquad \text{(A1)}$$

where $\vec{e}$ is the polarization of the light. In the case of the Mott excitations between the t_{2g} states, the current operator $\vec{J}$ is given by

$$\vec{J} = \sum_{m,n,\phi,\psi} i t_{m\phi n\psi} \vec{r}_{mn} (c^\dagger_{m\phi} c_{n\psi} - c^\dagger_{n\psi} c_{m\phi}), \qquad \text{(A2)}$$

where $t_{m\phi n\psi}$ is the transfer integral between the ϕ orbital of the t_{2g} states on the mth site and the ψ orbital on the nth site, and $\vec{r}_{mn}$ is the unit vector along the mth and nth sites. ϕ and ψ are d_{xy}, d_{yz}, or d_{zx}.

In the present model, we only consider the V t_{2g} states and the Coulomb interaction between the two electrons on the same V site but ignore the transfer of the electrons between the different V sites for considering the eigenstate of the d state. [We take account of the transfer in the current operator in Eq. (A2), though.] The final state $\langle f|$ is the one where an electron moves from one site (the A site) to another site (the B site) Accordingly, it is enough to take account of the "bond" composed of the A and B sites as $\langle f|$ and $|0\rangle$ in Eq. (A1), and to sum up the contribution of all the bonds to obtain the spectra for the whole crystal.

The eigenstates at each site are given by the multiplets of the d^n (t_{2g}^n) configuration, and can be represented by $|(d^n)^{2S+1}\Gamma(S_z)(\gamma)\rangle$, where S is the total spin, Γ (an irreducible representation of the symmetry) gives a set of the degenerate orbital states, S_z is the z component of the total spin, and γ specifies one orbital state, which is a basis of the irreducible presentation Γ.

Initially, there are two d electrons both at the A and B sites, and it is enough to consider the multiplets with the lowest energy for the d^2 configuration $^3T_1$ with the ninefold degeneracy (3 by the orbital and 3 by the spin; see also Appendix D). The energy of this $^3T_1$ state is $U' - J$, where U' is the Coulomb integral between different orbitals of the t_{2g} states, and J is the exchange integral for the t_{2g} states.

Thus, for the bond μ composed of the A and B sites, the initial state is given by

$$|0\rangle = \sum_{s,k,l} \xi(\mu,k,l)\alpha_s(\theta_\mu) \times |(d^2)^3T_1(S_z = s)(k) : A \bigotimes (d^2)^3T_1(S_z = 1)(l) : B\rangle, \qquad \text{(A3)}$$

where k and l are the orbital states of the A and B sites, respectively, and are the basis of the irreducible representation of T_1 ($d_{xy}d_{yz}$, $d_{zy}d_{zs}$, or $d_{zx}d_{xy}$). Here, we take the principal axis of the spins along the spin direction on the B site. Thus, S_z at the B site is fixed as 1. If the spin direction at the A site is θ_μ away from that at the B site, the electronic state at the A site is the superposition of the $S_z = 1$, 0, and -1 states, and $\alpha_s(\theta_\mu)$ ($s = 1,0,-1$) gives its coefficient. This $\alpha_s(\theta_\mu)$ can be determined by the generalized Pauli matrices for $S = 1$ spins.

On the other hand, the final states at the A and B sites are in the d^1 and d^3 configurations, respectively. The eigenstates of the d^1 configuration are ${}^2T_2$ with sixfold degeneracy (d_{xy}, d_{yz}, d_{zx}, $\overline{d_{xy}}$, $\overline{d_{yz}}$, and $\overline{d_{zx}}$, where $\overline{d_{xy}}$ means that the d_{xy} state is occupied by a down-spin electron). The eigenstates of the d^3 configuration are classified into four irreducible representations ${}^4A_2$ (fourfold degeneracy, energy $3U' - 3J$), ${}^2E$ (fourfold, $3U'$), ${}^2T_1$ (sixfold, energy $U + 2U' - 2J$), ${}^2T_2$ (sixfold, energy $U + 2U'$). Here, U is the Coulomb integral between the same orbitals of the t_{2g} states. For more details, see Appendix D.

Thus, the final state is given as follows:

$$\langle f| = \langle (d^1)^2 T_2(S_z = s')(i) : A \bigotimes (d^3)\Gamma(S_z = s + 1 - s')(j) : B|, \tag{A4}$$

where Γ is an irreducible representation of the multiplets for the d^3 configuration, and j is the orbital state of d^3, i.e., the basis for Γ. i is the orbital state of d^1. The sum $\sum_f$ in Eq. (A1) becomes $\sum_\Gamma \sum_{s',i,j}$ for one bond, and the summation of μ should be taken for the conductivity of the whole crystal.

The ε_f and ε_0 in Eq. (A1) is

$$\varepsilon_f = \varepsilon((d^3)\Gamma), \tag{A5}$$

$$\varepsilon_0 = 2\varepsilon((d^2)^3 T_1). \tag{A6}$$

Note that the energy of the state for the d^1 configuration is zero.

In the present compound, we take account of only a direct d-d transfer between the neighboring V sites, as shown in Fig. 5(b), and the magnitude of the transfer integral is assumed to be the same for all the possible transfers. Thus, as to the current operator $\vec{J}$ in Eq. (A2), ϕ should be the same as ψ, and if the bond μ is specified, only one ϕ has a nonzero transfer integral. For example, if the bond is on the xy plane, 45° away from the x axis ("xy bond"), only $\phi = d_{xy}$ has a nonzero transfer integral. Thus, $\vec{J}$ in Eq. (A1) can be replaced by

$$\vec{r_\mu} c^\dagger_{B\phi(\mu)} c_{A\phi(\mu)}. \tag{A7}$$

Therefore, the optical conductivity spectrum in the present compound is given as follows:

$$S_{\vec{e}}(\omega) = \sum_\Gamma I_{\vec{e}}(\Gamma)\delta\{\hbar\omega - [\varepsilon((d^3)\Gamma) - 2\varepsilon((d^2)^3 T_1)]\}, \tag{A8}$$

where $I_{\vec{e}}(\Gamma)$ is the spectral weight for the transition to the Γ state, and is given by

$$I_{\vec{e}}(\Gamma) = \sum_\mu \sum_{s',i,j} \sum_{s,k,l} |\xi(\mu,k,l)|^2 |\alpha_s(\theta_\mu)|^2 (\vec{e}\cdot\vec{r_\mu})^2 \times |M[\Gamma,s',i,j,s,k,l,\phi(\mu)]|^2. \tag{A9}$$

Here, $M[\Gamma,s',i,j,s,k,l,\phi(\mu)]$ is the matrix element of $\langle \ldots |$ in Eq. (A4) and $|\ldots\rangle$ in Eq. (A3) and the operator $c^\dagger_{B\phi(\mu)} c_{A\phi(\mu)}$ in-between.

The matrix element $M[\Gamma,s',i,j,s,k,l,\phi(\mu)]$ becomes the same for certain combinations of k, l (the orbital states at the A and B sites, respectively), and ϕ (the orbital state for the electronic transition). One is the case when an electron at the A site can move to the unoccupied state at the B site, for example, $k = d_{xy}d_{yz}$ and $l = d_{zx}d_{xy}$ and $\phi = d_{yz}$. We call this type of the orbital relation as a "P-type" orbital relation. Second is the case when an electron at the A site can move to an occupied state at the B site, for example, $k = d_{xy}d_{yz}$ and $l = d_{xy}d_{yz}$ and $\phi = d_{xy}$, which we call a "Q-type" orbital relation. The third is the case where no electron at the A site can move to the B site, for example, $k = d_{xy}d_{yz}$ and $l = d_{xy}d_{yz}$ and $\phi = d_{zx}$. In this case, the matrix element M is always zero.

Since any of the orbital relations for the nearest-neighbor V-V bonds in MnV_2O_4 that give a finite matrix element are either the P or Q type, we can replace the combination (k,l,ϕ) in the parentheses of M in Eq. (A9) by λ = P or Q. We also sum up $\xi(\mu,k,l)$ in Eq. (A9) as follows:

$$p(\mu,\lambda) = \sum_{[k,l,\phi(\mu)]\in\lambda} |\xi(\mu,k,l)|^2. \tag{A10}$$

With these, we can rewrite the expression of $I_{\vec{e}}(\Gamma)$ in Eq. (A9) as

$$I_{\vec{e}}(\Gamma) = \sum_\mu \sum_\lambda (\vec{e}\cdot\vec{r_\mu})^2 p(\mu,\lambda) I^\lambda_{\theta_\mu}(\Gamma), \tag{A11}$$

where

$$I^\lambda_{\theta_\mu}(\Gamma) = \sum_s \sum_{s',i,j} |\alpha_s(\theta_\mu)|^2 |M(\Gamma,s',i,j,s,\lambda)|^2. \tag{A12}$$

Here, $I^\lambda_{\theta_\mu}(\Gamma)$ gives the transition probability to the Γ state when the orbital relation is λ (= P or Q) type and the relative angles between the spins on the ends of the bonds (at the A and B sites) is θ_μ. $p(\mu,\lambda)$ gives the probability that the bond μ has a λ (= P or Q) type orbital relation.

APPENDIX B: CALCULATION OF THE TRANSITION PROBABILITY $I^\lambda_{\theta_\mu}(\Gamma)$

First, let us calculate $I^\lambda_{\theta_\mu}(\Gamma)$ in Eq. (A12), which is independent of the orbital ordering pattern. As described above, $\alpha_s(\theta)$ ($s = 1,0,-1$) corresponds to the coefficient of the $S_z = s$ state when the direction of the $S = 1$ spin is θ away from the z axis, and is given by the generalized Pauli matrices for $S = 1$ spins. Here, by rewriting $\alpha_{s=1}(\theta)$, $\alpha_{s=0}(\theta)$, and $\alpha_{s=-1}(\theta)$ as $\alpha(\theta)$, $\beta(\theta)$, and $\gamma(\theta)$, respectively, the specific formulas of them are given as shown in Eq. (3).

TABLE II. The value of $M(\Gamma,s',i,j,s,\lambda)$ for $\lambda = \mathrm{P}$ and $\Gamma = {}^4A_2$.

	$A_2^1\uparrow$	$A_2^1\downarrow$	$A_2^2\uparrow$	$A_2^2\downarrow$
$s=1$	1	0	0	0
$s=0$	0	$1/\sqrt{2}$	$1/\sqrt{6}$	0
$s=-1$	0	0	0	$1/\sqrt{3}$

Next, $|M(\Gamma,s',i,j,s,\lambda)|^2$ in Eq. (A12) can be calculated as follows: As an example of $\lambda = \mathrm{P}$, let us consider the case where the d_{xy} and d_{yz} states are occupied at the A site, the d_{zx} and d_{xy} states are occupied at the B site, and $\phi = d_{yz}$ [Fig. 5(c)]. The electron in the d_{yz} state at the A site can move to the B site, and as a result, the electronic state at the B site becomes $|d_{xy}d_{yz}d_{zx}|$ or $|d_{xy}\overline{d_{yz}}d_{zx}|$ (or the superposition of the two). This is not an eigenstate of the d^3 state but the superposition of them. The matrix element $M(\Gamma,s',i,j,s,\lambda)$ can be obtained by referencing Eqs. (D1), (D2), (D3), (D4), and (D5) below.

Here, we rewrite the final state, for example, $\langle(d^1)d_{xy} : A\bigotimes(d^3)A_2^1 : B|$, as $\Gamma^\tau\sigma = A_2^1\uparrow$, where $\sigma = \uparrow$ means that there is an up-spin electron left at the A site. The explicit forms of Γ^τ are shown in Appendix D. The table of $\lambda = \mathrm{P}$ for s (S_z of the A site in the initial state) in the first column versus $\Gamma^\tau\sigma$ ($\sigma = \uparrow$ or $\downarrow$) in the first line is shown in Tables II and III. The matrix elements with ${}^2T_1$ and ${}^2T_2$ are zero for $\lambda = \mathrm{P}$. Note that $\Gamma^\tau\sigma$ is given by Γ, $s+1-s'$ (S_z of the d^3 site), and j (the orbital state of the d^3 site), and σ is given by s' (S_z of the d^1 site), but i (the orbital state of the d^1 site) does not affect the value of $M(\Gamma,s',i,j,s,\lambda)$.

In a similar way, the table for $\lambda = \mathrm{Q}$ can be obtained and is shown in Table IV. The matrix elements with ${}^4A_2$ and ${}^2E$ are zero for $\lambda = \mathrm{Q}$. With these tables, Eq. (A12) can be calculated. The results are shown in Eq. (2).

APPENDIX C: CALCULATION OF THE PROBABILITY FOR THE P- AND Q-TYPE ORBITAL RELATION $p(\mu,\lambda)$ AND THE SPECTRAL WEIGHT $I_{\vec{e}}(\Gamma)$

$p(\mu,\lambda)$ given by Eq. (A10) is the probability that the bond μ has the λ-type orbital relation ($\lambda = \mathrm{P}$ or Q), and is dominated by the orbital-ordering pattern. Here, we discuss the orbital ordering where the probability of the orbital occupancy at each site is the one shown in Fig. 6.

As shown in Fig. 7, there are 8 out-of-plane bonds and 4 in-plane bonds (counting both the back and forth transition). Let us first discuss the 8 out-of-plane bonds. By seeing Figs. 5, 6, and 7, one notices that among $3\times 3 = 9$ possible pairs of the orbital states at the ends, there are 2 that become a P-type orbital relation both for the A→B transition ("out1" bond) and the B→A transition ("out2" bond), and the probability of the P-type for these two bonds is

$$p(\mathrm{out1},\mathrm{P}) + p(\mathrm{out2},\mathrm{P}) = 2b^2 + 2ab - a - 2b + 1. \quad \text{(C1)}$$

In a similar manner, we can calculate the probability of the Q-type orbital relation for the same bonds, which is given by the four possible pairs of the orbital states for both the A→B and B→A transitions, and the result is

$$p(\mathrm{out1},\mathrm{Q}) + p(\mathrm{out2},\mathrm{Q}) = -2b^2 - 2ab + 2a + 2b. \quad \text{(C2)}$$

The remaining $-a+1$ gives the probability of the orbital relation with zero matrix element M.

The angle between the spins on the ends of the out-of-plane bond is assumed as θ. Among the 8 out-of-plane bonds, 4 are the out1 bonds and the remaining 4 are the out2 bonds. As to $(\vec{e}\cdot\vec{r_\mu})^2$, when $\vec{e}$ is along the x axis, $(\vec{e}\cdot\vec{r_\mu})^2 = \frac{1}{2}$ for half bonds and $(\vec{e}\cdot\vec{r_\mu})^2 = 0$ for the remaining half. When $\vec{e}$ is along the z axis, $(\vec{e}\cdot\vec{r_\mu})^2 = \frac{1}{2}$ for all the bonds [see Fig. 7(a)].

Next, let us discuss the 4 in-plane bonds. By a similar discussion for the out-of-plane bonds, the probability of the P-type orbital relation is

$$2p(\mathrm{in},\mathrm{P}) = -2a^2 + 2a, \quad \text{(C3)}$$

and the probability of the Q type is

$$2p(\mathrm{in},\mathrm{Q}) = 2a^2 - 4a + 2. \quad \text{(C4)}$$

The remaining $2a$ corresponds to the probability giving zero matrix element.

The angle between the spins on the ends of the in-plane bond is assumed as θ'. As to $(\vec{e}\cdot\vec{r_\mu})^2$, when $\vec{e}$ is along the x axis, $(\vec{e}\cdot\vec{r_\mu})^2$ is always $\frac{1}{2}$ for all the 4 in-plane bonds, and when $\vec{e}$ is along the z axis, $(\vec{e}\cdot\vec{r_\mu})^2$ is always zero [Fig. 7(b)].

Thus, Eq. (A11) with $\vec{e}\parallel x$ and $\vec{e}\parallel z$ can be written as follows:

$$I_x(\Gamma) = \sum_{\lambda=\mathrm{P,Q}} 2\times\frac{1}{2}\times[p(\mathrm{out1},\lambda) + p(\mathrm{out2},\lambda)]I_\theta^\lambda(\Gamma) + 4\times\frac{1}{2}\times p(\mathrm{in},\lambda)I_{\theta'}^\lambda(\Gamma), \quad \text{(C5)}$$

$$I_z(\Gamma) = \sum_{\lambda=\mathrm{P,Q}} 4\times\frac{1}{2}\times[p(\mathrm{out1},\lambda) + p(\mathrm{out2},\lambda)]I_\theta^\lambda(\Gamma). \quad \text{(C6)}$$

Specific formulas for the ${}^4A_2$ and ${}^2E$ modes can be obtained by substituting Eqs. (2), (C1), (C2), (C3), and (C4) for Eqs. (C5) and (C6):

$$I_x({}^4A_2) = (2b^2+2ab-a-2b+1)\left(\alpha^2+\frac{2}{3}\beta^2+\frac{1}{3}\gamma^2\right) + (-2a^2+2a)\left(\alpha'^2+\frac{2}{3}\beta'^2+\frac{1}{3}\gamma'^2\right),$$

TABLE III. The value of $M(\Gamma,s',i,j,s,\lambda)$ for $\lambda = \mathrm{P}$ and $\Gamma = {}^2E$.

	$E^1\uparrow$	$E^1\downarrow$	$E^2\uparrow$	$E^2\downarrow$
$s=1$	0	0	0	0
$s=0$	$1/2$	0	$-1/2\sqrt{3}$	0
$s=-1$	0	$1/\sqrt{2}$	0	$-1/\sqrt{6}$

TABLE IV. The value of $M(\Gamma,s',i,j,s,\lambda)$ for $\lambda = \mathrm{Q}$.

	$T_1^2\uparrow$	$T_1^2\downarrow$	$T_2^2\uparrow$	$T_2^2\downarrow$
$s=1$	0	0	0	0
$s=0$	$-1/2$	0	$1/2$	0
$s=-1$	0	$-1/\sqrt{2}$	0	$1/\sqrt{2}$

$$
\begin{aligned}
I_x(^2E) &= (2b^2+2ab-a-2b+1)\left(\frac{1}{3}\beta^2+\frac{2}{3}\gamma^2\right)\\
&\quad+(-2a^2+2a)\left(\frac{1}{3}\beta'^2+\frac{2}{3}\gamma'^2\right),\\
I_z(^4A_2) &= 2(2b^2+2ab-a-2b+1)\left(\alpha^2+\frac{2}{3}\beta^2+\frac{1}{3}\gamma^2\right),\\
I_x(^2E) &= 2(2b^2+2ab-a-2b+1)\left(\frac{1}{3}\beta^2+\frac{2}{3}\gamma^2\right),
\end{aligned}
\tag{C7}
$$

where $\alpha=\alpha(\theta)$ and $\alpha'=\alpha(\theta')$, etc.

APPENDIX D: ELECTRONIC STATES FOR d^2 AND d^3 CONFIGURATIONS IN THE t_{2g} STATES

In this section, the explicit form of each multiplet is shown by a Slater determinant.[32] There are ${}_6C_2=15$ states for the d^2 configuration in the t_{2g} states, and those are classified into four eigenstates (multiplets) with the following irreducible representations: $^3T_1$ (ninefold degeneracy, energy $U'-J$), ^1E (twofold, $U-J$), $^1T_2$ (fourfold, $U'+J$), and $^1A_1$ (nondegenerate, $U+2J$). It is enough to take account of the state with the lowest energy $^3T_1$ here. The nine states for the $^3T_1$ states can be written as follows:

$$
\begin{array}{lll}
S_z=1 & S_z=0 & S_z=-1\\
|d_{xy}d_{yz}|, & \frac{1}{\sqrt{2}}(|d_{xy}\overline{d_{yz}}|+|\overline{d_{xy}}d_{yz}|), & |\overline{d_{xy}d_{yz}}|\\
|d_{yz}d_{zx}|, & \frac{1}{\sqrt{2}}(|d_{yz}\overline{d_{zx}}|+|\overline{d_{yz}}d_{zx}|), & |\overline{d_{yz}d_{zx}}|\\
|d_{zx}d_{xy}|, & \frac{1}{\sqrt{2}}(|d_{zx}\overline{d_{xy}}|+|\overline{d_{zx}}d_{xy}|), & |\overline{d_{zx}d_{xy}}|.
\end{array}
\tag{D1}
$$

On the other hand, there are ${}_6C_3=20$ states for the d^3 configuration in the t_{2g} states, and those are classified into four eigenstates with the following irreducible representations: $^4A_2$ (fourfold degeneracy, energy $3U'-3J$), ^2E (fourfold, $3U'$), $^2T_1$ (sixfold, energy $U+2U'-2J$), and $^2T_2$ (sixfold, energy $U+2U'$). Each state can be written as follows, where the state $|(d^n)^{2S+1}\Gamma(S_z)(\gamma)\rangle$ is rewritten as Γ^τ, where τ represents (S_z,γ):

$$
\begin{array}{ll}
^4A_2 \quad (3U'-3J) & \\
|d_{xy}d_{yz}d_{zx}|, & A_2^1\\
\frac{1}{\sqrt{3}}(|\overline{d_{xy}}d_{yz}d_{zx}|+|d_{xy}\overline{d_{yz}}d_{zx}|+|d_{xy}d_{yz}\overline{d_{zx}}|), & A_2^2\\
\frac{1}{\sqrt{3}}(|d_{xy}\overline{d_{yz}d_{zx}}|+|\overline{d_{xy}}d_{yz}\overline{d_{zx}}|+|\overline{d_{xy}d_{yz}}d_{zx}|), & A_2^3\\
|\overline{d_{xy}d_{yz}d_{zx}}|, & A_2^4
\end{array}
\tag{D2}
$$

$$
\begin{array}{ll}
^2E \quad (3U') & \\
\frac{1}{\sqrt{2}}(|d_{xy}\overline{d_{yz}}d_{zx}|-|\overline{d_{xy}}d_{yz}d_{zx}|), & E^1\\
\frac{1}{\sqrt{6}}(2|d_{xy}d_{yz}\overline{d_{zx}}|-|d_{xy}\overline{d_{yz}}d_{zx}|-|\overline{d_{xy}}d_{yz}d_{zx}|), & E^2\\
\frac{1}{\sqrt{2}}(|\overline{d_{xy}}d_{yz}\overline{d_{zx}}|-|d_{xy}\overline{d_{yz}d_{zx}}|), & E^3\\
\frac{1}{\sqrt{6}}(2|\overline{d_{xy}d_{yz}}d_{zx}|-|\overline{d_{xy}}d_{yz}\overline{d_{zx}}|-|d_{xy}\overline{d_{yz}d_{zx}}|), & E^4
\end{array}
\tag{D3}
$$

$$
\begin{array}{ll}
^2T_1 \quad (U+2U'-2J) & \\
\frac{1}{\sqrt{2}}(|d_{xy}d_{yz}\overline{d_{yz}}|-|d_{xy}d_{zx}\overline{d_{zx}}|), & T_1{}^1\\
\frac{1}{\sqrt{2}}(|d_{yz}d_{zx}\overline{d_{zx}}|-|d_{yz}d_{xy}\overline{d_{xy}}|), & T_1{}^2\\
\frac{1}{\sqrt{2}}(|d_{zx}d_{xy}\overline{d_{xy}}|-|d_{zx}d_{yz}\overline{d_{yz}}|), & T_1{}^3\\
\frac{1}{\sqrt{2}}(|\overline{d_{xy}d_{yz}}d_{yz}|-|\overline{d_{xy}d_{zx}}d_{zx}|), & T_1{}^4\\
\frac{1}{\sqrt{2}}(|\overline{d_{yz}d_{zx}}d_{zx}|-|\overline{d_{yz}d_{xy}}d_{xy}|), & T_1{}^5\\
\frac{1}{\sqrt{2}}(|\overline{d_{zx}d_{xy}}d_{xy}|-|\overline{d_{zx}d_{yz}}d_{yz}|), & T_1{}^6
\end{array}
\tag{D4}
$$

$$
\begin{array}{ll}
^2T_2 \quad (U+2U') & \\
\frac{1}{\sqrt{2}}(|d_{xy}d_{yz}\overline{d_{yz}}|+|d_{xy}d_{zx}\overline{d_{zx}}|), & T_2{}^1\\
\frac{1}{\sqrt{2}}(|d_{yz}d_{zx}\overline{d_{zx}}|+|d_{yz}d_{xy}\overline{d_{xy}}|), & T_2{}^2\\
\frac{1}{\sqrt{2}}(|d_{zx}d_{xy}\overline{d_{xy}}|+|d_{zx}d_{yz}\overline{d_{yz}}|), & T_2{}^3\\
\frac{1}{\sqrt{2}}(|\overline{d_{xy}d_{yz}}d_{yz}|+|\overline{d_{xy}d_{zx}}d_{zx}|), & T_2{}^4\\
\frac{1}{\sqrt{2}}(|\overline{d_{yz}d_{zx}}d_{zx}|+|\overline{d_{yz}d_{xy}}d_{xy}|), & T_2{}^5\\
\frac{1}{\sqrt{2}}(|\overline{d_{zx}d_{xy}}d_{xy}|+|\overline{d_{zx}d_{yz}}d_{yz}|), & T_2{}^6
\end{array}
\tag{D5}
$$

Note that the A_2^1, A_2^2, A_2^3, and A_2^4 states are the $S_z=\frac{3}{2}$, $\frac{1}{2}$, $-\frac{1}{2}$, and $-\frac{3}{2}$ states, respectively, and for each of the ^2E, T_1, and T_2 states, the former half are the $S_z=\frac{1}{2}$ states and the latter half are the $S_z=-\frac{1}{2}$ states.

*katsuf@waseda.jp
†Present address: Department of Physics and Astronomy, University of British Columbia.
‡Present address: Cross-Correlated Materials Research Group (CMRG), RIKEN Advanced Science Institute.

[1] A. J. Millis, Nature (London) **392**, 147 (1998).

[2]Y. Murakami, J. P. Hill, D. Gibbs, M. Blume, I. Koyama, M.Tanaka, H. Kawata, T. Arima, Y. Tokura, K. Hirota, and Y. Endoh, Phys. Rev. Lett. **81**, 582 (1998).
[3]Y. Ren, T. T. M. Palstra, D. I. Khomskii, E. Pellegrin, A. A. Nugroho, A. A. Menovsky, and G. A. Sawatzky, Nature (London) **396**, 441 (1998).
[4]M. Noguchi, A. Nakazawa, S. Oka, T. Arima, Y. Wakabayashi, H. Nakao, and Y. Murakami, Phys. Rev. B **62**, R9271 (2000).
[5]Y. Ueda, N. Fujiwara, and H. Yasuoka, J. Phys. Soc. Jpn. **66**, 778 (1997).
[6]S.-H. Lee, D. Louca, H. Ueda, S. Park, T. J. Sato, M. Isobe, Y. Ueda, S. Rosenkranz, P. Zschack, J. Íñiguez, Y. Qiu, and R. Osborn, Phys. Rev. Lett. **93**, 156407 (2004).
[7]K. Adachi, T. Suzuki, K. Kato, K. Osaka, M. Takata, and T. Katsufuji, Phys. Rev. Lett. **95**, 197202 (2005).
[8]T. Suzuki, M. Katsumura, K. Taniguchi, T. Arima, and T. Katsufuji, Phys. Rev. Lett. **98**, 127203 (2007).
[9]V. O. Garlea, R. Jin, D. Mandrus, B. Roessli, Q. Huang, M. Miller, A. J. Schultz, and S. E. Nagler, Phys. Rev. Lett. **100**, 066404 (2008).
[10]J. H. Chung, J. H. Kim, S. H. Lee, T. J. Sato, T. Suzuki, M. Katsumura, and T. Katsufuji, Phys. Rev. B **77**, 054412 (2008).
[11]E. M. Wheeler, B. Lake, A. T. M. Nazmul Islam, M. Reehuis, P. Steffens, T. Guidi, and A. H. Hill, Phys. Rev. B **82**, 140406(R) (2010).
[12]G. Giovannetti, A. Stroppa, S. Picozzi, D. Baldomir, V. Pardo, S. Blanco-Canosa, F. Rivadulla, S. Jodlauk, D. Niermann, J. Rohrkamp *et al.* , Phys. Rev. B **83**, 060402(R) (2011).
[13]T. Katsufuji, T. Suzuki, H. Takei, M. Shingu, K. Kato, K. Osaka, M. Takata, H. Sagayama, and T. Arima, J. Phys. Soc. Jpn. **77**, 053708 (2008).
[14]J. S. Lee, Y. S. Lee, T. W. Noh, S.-J. Oh, J. Yu, S. Nakatsuji, H. Fukazawa, and Y. Maeno, Phys. Rev. Lett. **89**, 257402 (2002).
[15]S. Miyasaka, Y. Okimoto, and Y. Tokura, J. Phys. Soc. Jpn. **71**, 2086 (2002).
[16]A. A. Tsvetkov, F. P. Mena, P. H. M. van Loosdrecht, D. van der Marel, Y. Ren, A. A. Nugroho, A. A. Menovsky, I. S. Elfimov, and G. A. Sawatzky, Phys. Rev. B **69**, 075110 (2004).
[17]E. Benckiser, R. Rückamp, T. Möller, T. Taetz, A. Möller, A. A. Nugroho, T. T. M. Palstra, G. S. Uhrig, and M. Grüninger, New J. Phys. **10**, 053027 (2008).
[18]J. Reul, A. A. Nugroho, T. T. M. Palstra, and M. Grüninger, Phys. Rev. B **86**, 125128 (2012).
[19]K. Tobe, T. Kimura, Y. Okimoto, and Y. Tokura, Phys. Rev. B **64**, 184421 (2001).
[20]J. S. Lee, M. W. Kim, and T. W. Noh, New J. Phys. **7**, 147 (2005).
[21]M. M. Qazilbash, A. A. Schafgans, K. S. Burch, S. J. Yun, B. G. Chae, B. J. Kim, H. T. Kim, and D. N. Basov, Phys. Rev. B **77**, 115121 (2008).
[22]M. K. Stewart, D. Brownstead, S. Wang, K. G. West, J. G. Ramirez, M. M. Qazilbash, N. B. Perkins, I. K. Schuller, and D. N. Basov, Phys. Rev. B **85**, 205113 (2012).
[23]A. Gössling, R. Schmitz, H. Roth, M. W. Haverkort, T. Lorenz, J. A. Mydosh, E. Müller-Hartmann, and M. Grüninger, Phys. Rev. B **78**, 075122 (2008).
[24]S. J. Moon, W. S. Choi, S. J. Kim, Y. S. Lee, P. G. Khalifah, D. Mandrus, and T. W. Noh, Phys. Rev. Lett. **100**, 116404 (2008).
[25]S. J. Moon, H. Jin, W. S. Choi, J. S. Lee, S. S. A. Seo, J. Yu, G. Cao,, T. W. Noh, and Y. S. Lee, Phys. Rev. B **80**, 195110 (2009).
[26]H. Tsunetsugu and Y. Motome, Phys. Rev. B **68**, 060405 (2003).
[27]O. Tchernyshyov, Phys. Rev. Lett. **93**, 157206 (2004).
[28]S. Sarkar, T. Maitra, R. Valentí, and T. Saha-Dasgupta, Phys. Rev. Lett. **102**, 216405 (2009).
[29]G.-W. Chern, N. Perkins, and Z. Hao, Phys. Rev. B **81**, 125127 (2010).
[30]K. Takenaka, K. Iida, Y. Sawaki, S. Sugai, Y. Moritomo, and A. Nakamura, J. Phys. Soc. Jpn. **68**, 1828 (1999).
[31]The fact that two Lorentzians are necessary to fit the overall feature of the 1.6-eV peak does not necessarily mean that there are two excitations for the 1.6-eV peak, but should be regarded as the practical way of the fitting for the spectra that deviates from a single Lorentzian because of a dispersion of the excitation.
[32]Y. Tanabe, S. Sugano, and H. Kamimura, *Multiplets of Transition-Metal Ions in Crystals* (Academic, New York, 1970).
[33]T. Tohyama, Phys. Rev. B **70**, 174517 (2004).